Z. Kristallogr. **222** (2007) 605–611 / **DOI** 10.1524/zkri.2007.222.11.605

Solving the 3D structure of metal nanoparticles

Anatoly Frenkel*

Physics Department, Yeshiva University, 245 Lexington Avenue, New York, NY 10016, USA

Received March 3, 2007; accepted July 23, 2007

Nanoparticles / Nanoalloys / EXAFS / Structure analysis / Short range order

Abstract. We discuss methods of Extended X-ray Absorption Fine-Structure (EXAFS) analysis that provide three-dimensional structural characterization of metal nanoparticles, both mono- and bi-metallic. For the bimetallic alloys, we use short range order measurements to discriminate between random and non-random inter-particle distributions of atoms. We also discuss the application of EXAFS to heterogeneous nanoparticle systems.

Introduction

The question of the fundamental interest in structural studies of nanoparticles and their applications, *e.g.*, to catalysis, is how to reconstruct their structure and geometry from experiment. Scattering methods (X-ray, neutron, electron diffraction) can reconstruct 3D arrangement of atoms in nanoparticles that formed single crystals. Such studies can probe structure in particles with as few as 13 atoms [1]. To reconstruct 3D geometry in isolated particles, several methods exist which have been applied, however, to relatively large particles (>3–4 nm in diameter). Among them are electron microscopies (TEM/STEM and HRTEM) that report particle size and its distribution, electron and X-ray diffraction, including recently developed atomic pair distribution function methods [2], that index nanocrystalline structure, energy-dispersive X-ray analysis (EDX), that measures compositional distribution, etc. However, the accuracy and the level of detail decrease for smaller particles, rendering traditional methods ineffective for sizes of the order of 1–2 nm or less.

During the last decate, a high-angle annular dark field scanning TEM (HAADF-STEM, also known as the "Z-contrast") technique has been employed to count the number of atoms in the nanoparticles [3], study particle geometry and nanoalloy composition [4]. Using this method, it was possible to obtain the number of atoms (with the uncertainty of $\pm$ 2 atoms) in the unsupported, ligand protected 13-atom Au clusters [5], as well as supported (γ-Al_2O_3) 12-atom Pt clusters [6].

Due to their non-bulk properties, inherently small length scale, the lack of the long range order, only a combination of different structural techniques can bring enough characterization power to decipher the structure of nanoparticles in sub-nm to 2–3 nm size range. Extended X-ray absorption fine-structure (EXAFS) spectroscopy is one of the premiere tools to study atomic structure of nanoparticles. Soon after EXAFS was first introduced by Stern, Sayers and Lytle as a structural technique [7], its potential in solving the structure of nanoparticles was recognized by Sinfelt, Via, Meitzner, *et al.* [8]. Indeed, EXAFS directly measures real-space, structural information which is virtually instantaneous (the characteristic time of the photoelectron interference effect is ca. 10^{-15} s) and local (only distances within 6–8 Å away from the absorbing atoms can be probed).

The EXAFS signal, $\chi(k)$, is the sum of all contributions, $\chi_i(k)$, from groups of neighbors at approximately equal distances from the absorbing atoms (*i.e.*, the *i*-th shell), which are often written as [9]:

$$\chi_i(k) = \frac{S_0^2 n_i}{kR_i^2}\left|f_i^{\mathrm{eff}}(k)\right| \times \sin\left[2kR_i - \frac{4}{3}\,\sigma_i^{(3)}k^3 + \delta_i(k)\right]\mathrm{e}^{-2\sigma_i^2 k^3}\,\mathrm{e}^{-2R_i/\lambda_i(k)},$$

where k is the photoelectron wave number, $f_i^{\mathrm{eff}}(k)$ and $\delta_i(k)$ are the photoelectron scattering-path amplitude and phase, respectively, S_0^2 is the passive electron reduction factor, n_i is the degenacy of the scattering path, R_i is the effective half-path-length (which is equal to the interatomic distance for single-scattering paths), σ_i^2 is the mean-square deviation in R_i, $\sigma_i^{(3)}$ is the third cumulant, and $\lambda_i(k)$ is the photoelectron mean free path. Using modern computer packages, *e.g.*, IFEFFIT [10], which employs a non-linear least square method to fit theoretically calculated (with the help of FEFF6 code [9]) EXAFS signal to the data, the best-fit values of structural parameters can be obtained, together with their uncertainties.

One of the reasons EXAFS is a method of choice for nanoparticle studies is the local range (within ca. 8 Å) where this technique probes the structure around absorbing atoms and its sensitivity to the partial radial distribution function $\varrho_{AB}(r)$ of atoms B which are neighbors to the absorbing atom A. The changes in $\varrho_{AB}(r)$ can be particularly dramatic between the nanoparticles and their bulk counterparts due to the finite size effects. For example, metal-metal coordination numbers and distances in clusters

* e-mail: Anatoly.Frenkel@yu.edu

are different from the bulk. Furthermore, proximity of most of the atoms to the nanocluster surface and/or the substrate contributes to the total bond length disorder (σ^2). Effects of alloying (presence or absence of the short range order) in bimetallic clusters can be examined by studying metal-metal partial coordination numbers and bond buckling. In the following sections, we will describe several modeling strategies that are useful for the nanoparticles structure analysis by EXAFS.

Geometry and short range order

We will limit the scope of this section to supported clusters and monolayer protected clusters. Such nanoparticles, both monometallic (Pt, Pd, Au, Co, Rh, Ni, etc.) and alloys (Pt/Ru, Au/Pd, Pd/Cu, Ni/Pt, Ag/Pd, etc.) can be prepared by a variety of synthetic methods for a large number of support materials and ligands. They possess high degree of symmetry, their size and properties can be controlleld by synthetic conditions which use various supports and ligands, and, therefore, offer good test cases for technique development. The closed shell clusters are characterized by "magic numbers" of atoms, which are unique for a given family of clusters. Many types of the closed shell, regular polyhedral clusters (cuboctahedral and icosahedral [11], truncated decahedral [12], truncated octahedral [13], hexagonal closed packed [14], etc.) have long been proposed, to be energetically most stable [15, 16]. Mapping these geometries, which are often conflicting [17], to a particular system is very difficult due to the lack of an adequate experimental protocol that would measure relevant geometrical properties of the clusters.

In this section we will outline methods of EXAFS data analysis, developed in recent years, that allow to obtain quantitative geometric characteristics of monodisperse nanoparticles. For monometallic nanoparticles, we will show how to discriminate between models differing in the manner of atomic packing (closed packed v. non-closed packed) and/or morphology (*e.g.*, cuboctahedral v. octahedral). Combined with the particle size determination, this level of detail allows to reconstruct 3D atomic structure of the clusters. For bimetallic clusters, in addition to the size/shape determination, we will be able to discriminate between random and non-random alloying of metals. For non-random alloys, we will characterize the short range order around each absorber in terms of the positive or negative tendency of like atoms to cluster and/or form a core/shell type nanoalloy.

Monometallic nanoparticles

In the case of single-scattering (SS) paths, n_i in EXAFS equation above is a coordination number of atoms in the i-th coordination shell, and R_i – interatomic distance between the central atom and its i-th nearest neighbor. In many cases when the mononetallic nanoparticles are symmetrically surrounded by ligands, or when they as colloids in solutions, or stabilized by dendrimers, a regular polyhedron is a good approximation for a nanocluster. While such approximation is justified for relatively small clusters (between 10 and 1000 atoms) where many stable isomers have competing total energies and thus can all contribute to the energy landscape at the nanoscale, at the larger sizes, *i.e.*, where the details of surface morphology of different isomers do not significantly affect cluster energy, a simple "sphere" becomes an efficient model.

Both approaches allow to obtain the first nearest neighbor coordination numbers (1 NN) n_1 for regular clusters. Using the first approach, Montejano-Carrizales, *et al.* [18], studied geometrical characteristic of several regular polyhedral clusters (cubo-octahedral, icosahedral, body-centered cubic and simple cubic) analytically as a function of the cluster order L. Defining $L = N_E - 1$, where N_E is the number of atoms along the edge of a regular polyhedron, the following relationships can be derived for the 1 NN coordination numbers in cuboctahedral (closed packed) and icosahedral (non-closed packed) clusters that have the same sequence of their magic numbers ($N = 13$, 55, 147, 309, 561, 923 ...) [18]:

$$n_1^{co} = \frac{24L(5L^2 + 3L + 1)}{10L^3 + 15L^2 + 11L + 3}, \qquad n_1^{i\cos} = \frac{6L(20L^2 + 15L + 7)}{10L^3 + 15L^2 + 11L + 3}. \tag{1}$$

Calvin, *et al.* [19], used the second approach by approximating the cluster shape as a sphere with radius R and obtaining the 1 NN coordination number for a cluster with average 1 NN distance r as follows:

$$n_1 \approx \left[1 - \frac{3}{4}\left(\frac{r}{R}\right) + \frac{1}{16}\left(\frac{r}{R}\right)^3\right] n_1^{\text{bulk}}.$$

This approach is advantageous for larger clusters, and when the size distribution is relatively broad. Since for the cuboctahedral clusters, $R = Lr$, and $n_1^{\text{bulk}} = 12$, we obtain:

$$n_1^{\text{co}} \approx 12\left[1 - \frac{3}{4}\left(\frac{1}{L}\right) + \frac{1}{16}\left(\frac{1}{L}\right)^3\right]. \tag{2}$$

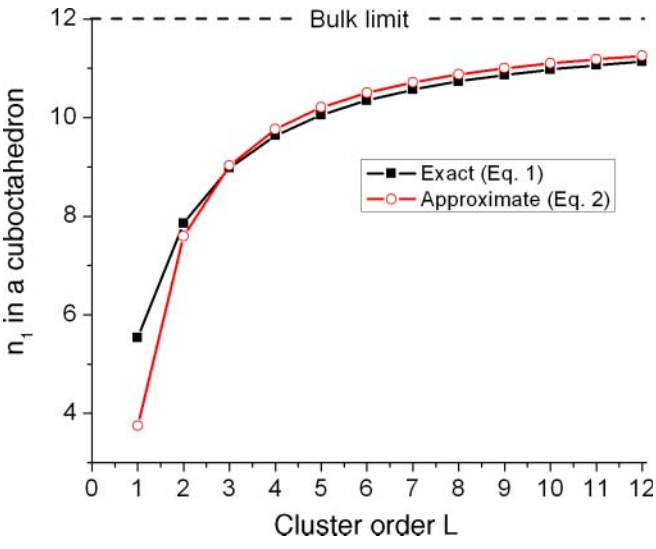

Fig. 1. Comparison of the exact (Ref. 18) and approximate (Ref. 19) methods of calculating the 1NN coordination number in cuboctahedral clusters.

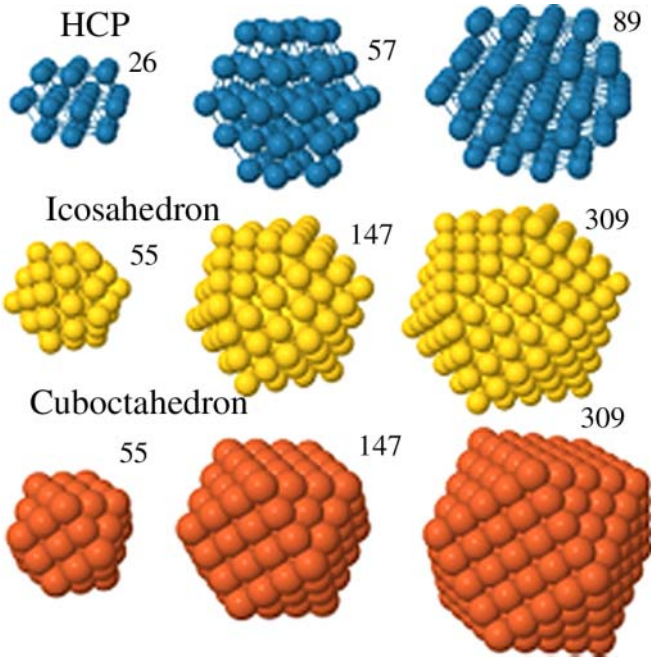

Fig. 2. Atomic configurations and magic numbers for several representative clusters.

Figure 2 demonstrates that Eq. (2) is in a reasonable agreement with Eq. (1) for $L = 3$ and higher, *i.e.*, when number of atoms in the cluster is > 100.

The methods describe above based on analytical calculations of the coordination numbers and working well for calculating n_1 to any order, are not efficient for the coordination numbers, corresponding to the more distant shells: n_2, n_3, n_4, ... Since multiple-scattering contribution to EXAFS in nanoclusters can be quantitatively analyzed [20], not only the single-scattering coordination numbers but also multiple-scattering path degeneracies could be reliably extracted from the EXAFS data. Such additional information effectively communicates size, shape and surface orientation of nanoclusters [21].

Due to the large variety of these indices, their analytical estimation as a function of cluster order is not practical. Indeed, not only such indices are unique for specific cluster geometries (cuboctahedral, icosahedral, hexagonal closed packed, etc.), they need to be also generated for truncated clusters that simulate supported nanoparticles. We adopted a different approach by developing a suite of programs that generate these indices for a given cluster geometry (Fig. 2) [22].

For a cluster of N identical atoms, we compute cluster-average pair radial distribution function $\varrho(r)$, or RDF, as follows:

$$\varrho(r) = \frac{1}{N}\sum_{i=1}^{N} \varrho_i(r)\,, \qquad \varrho_i(r) = \frac{\mathrm{d}N_i}{\mathrm{d}R_i}\,,$$

where $\varrho_i(r)$ is a partial RDF for an atom i, and $\mathrm{d}N_i$ is the number of its neighbors within the spherical shell of thickness $\mathrm{d}R_i$. Coordination numbers within a given shell (between R_1 and R_2) in model clusters can be obtained as:

$$n_i = \int_{R_1}^{R_2} \varrho(r)\,\mathrm{d}r\,, \qquad (3)$$

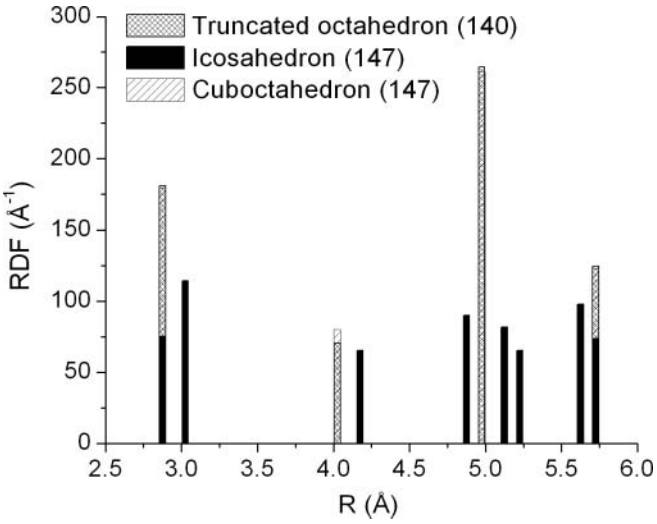

Fig. 3. RDF histograms calculated for a truncated octahedron (140 atoms), icosahedron (147) and a cuboctahedron (147). In all cases, $r = 2.87$ Å.

and be directly compared with those measured by EXAFS.[1] To demonstrate the role of the coordination numbers for the cluster geometry characterization, we plot the histogram of the RDF (with bin size of 0.05 Å) for truncated octahedral, icosahedral and cuboctahedral clusters (Fig. 3). The 1 NN distance r was chosen to be 2.87 Å in all cases. Figure 3 demonstrates the effect of the icosahedral strain (5%) on the coordination shells 1 through 4, and the similarity between the RDF's of the two closed packed structures. Only detecting the small difference in the intensity of the second nearest neighbor peak would allow one to discriminate between these two very similar models that coincide for the Au_{13} clusters as described below.

Recent HAADF-STEM-EXAFS analyses of highly monodispersed, mixed-ligand Au_{13} clusters [23] demonstrated the predictive power of the RDF method. Indeed, $n_2 = 0$ for a 13 atom icosahedron, while $n_2 = 1.85$ for a 13 atom cuboctahedron (same for the truncated octahedron which is isostructural to the cuboctahedron for 13 atom clusters). Figure 4 shows that the icosahedral model for the mixed-ligand Au_{13} cluster is preferred to the alternative one, modeled as a closed packed 13-atom cluster, given the agreement of the experimentally obtained 1 NN, 2 NN and 3 NN coordination numbers [23] with the former model, while the latter model differs from the data (the most dramatic is the difference in n_2). Thus, accurate measurement of these indices in monodispersed clusters can allow to discriminate between different structures for larger clusters where the higher order neighbors are detectable by EXAFS.

Bimetallic nanoparticles

In homogeneous samples (with narrow size and compositional distributions over the particles), there are two distinctly different types of mixing of A and B atoms. They

[1] Cluster coordinates for many different types of regular and truncated polyhedral clusters can be obtained by contacting the author. They are also available from: http://www.yu.edu/scc.

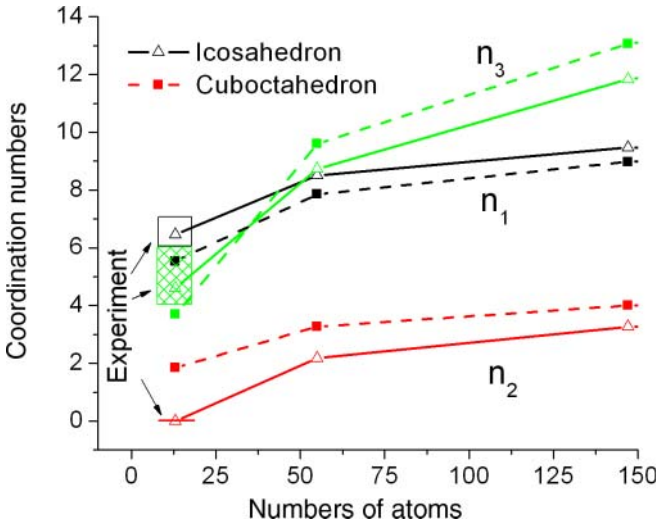

Fig. 4. Experimental results (Ref. [23]) vs. model calculations [24] of the 1NN, 2NN and 3NN coordination numbers for icosahedral and cuboctahedral clusters.

can be mixed statistically (*i.e.*, randomly, in accordance with the overall concentration) or non-statistically. The most common example of non-statistical mixing is segregation of atoms of different elements, forming a "core-shell" type particle where larger than the concentration-weighted average number of atoms of one type can be found in the core, and the other type – at the surface of the particle. In heterogeneous samples, where different clusters (*A*-rich and *B*-rich) can be formed, the situation may be further complicated [25].

For *random* alloys, the average coordination numbers n_{AA} and n_{AB} of A and B atoms relative to A atom are in the same proportion as the bulk concentrations of these elements in the sample:

$$\frac{n_{AA}}{n_{AB}} = \frac{x_A}{x_B} .$$

For alloys with nonzero short range order, the left part may be *larger* or *smaller* than the right part, indicating *positive* or *negative* tendency to clustering, respectively. In the former case, the atoms A and B segregate to different regions of the nanoalloy. In the latter, the A atoms are preferentially coordinated with B (with probability greater than x_A/x_B) and vice versa.

We can also introduce a short range order parameter, α, analogously to its definition by Cowley for bulk alloys [26]:

$$\alpha = 1 - \frac{n_{AB}/n_{AM}}{x_B} ,$$

where $n_{AM} = n_{AA} + n_{AB}$ is the coordination number of the *A*-metal bonds. For alloys with positive and negative tendency to clustering, α will be positive or negative, respectively. However, even after the segregation is demonstrated by examining the experimental values of n_{AA}/n_{AB} or α, more experimental information is still needed to find out whether *A* is predominantly in the surface or in the core, as well as for the determination of the particle size.

Such information is available by measuring EXAFS on both A and B central atoms and extracting coordination numbers n_{AA}, n_{AB} and n_{BB}. The analysis should be done concurrently, with obvious constraints imposed on the heterometallic bonds during the fits [27]:

$$n_{AB} = \frac{x_B}{x_A} n_{BA} , \tag{3}$$

$$R_{AB} = R_{BA} , \qquad \sigma^2_{AB} = \sigma^2_{BA} . \tag{4}$$

The atoms of the type *A* will segregate to the surface of the nanoparticle and *B* – to the core, if $n_{AM} < n_{BM}$, since atoms at the surface have fewer neighbors than those in the core. This criterion is useful even for alloys containing elements that are neighbors in periodic table (*e.g.*, Fe–Ni, Pd–Ag, etc.) where only the total n_{AM}, n_{BM} numbers can be measured by EXAFS analysis of *A* and *B* absorbing atoms, respectively, due to the similarity of backscattering amplitudes of *A*–*A* and *A*–*B* pairs (as well as *B*–*A* and *B*–*B*).

Another advantage of analyzing both *A* and *B* EXAFS data is for the particle geometry determination. Indeed, the average number of metal-metal neighbors per metal atom:

$$n_{MM} = x_A n_{AM} + x_B n_{BM} . \tag{5}$$

for the first nearest neighbor shell, combined with other information (*e.g.*, higher shell coordination numbers, TEM data, etc.) allows to estimate the particle size by methods similar to those described above for monometallic particles.

Random bimetallic alloys have a unique behavior of these coordination numbers with concentration. Assume, for simplicity, a bimetallic nanoparticle of a certain size, with random distribution of *A* and *B* atoms, where the following relationships apply:

$$n_{AM} = n_{BM} = n_{MM} , \tag{6}$$

$$n_{AA} = n_{BA} = x_A n_{MM} , \tag{7}$$

$$n_{BB} = n_{AB} = x_B n_{MM} = (1 - x_A)\, n_{MM} . \tag{8}$$

Thus, partial coordination numbers should depend *linearly* on alloy concentration (Fig. 5) in *random* nanoalloys, provided that the particle size is the same at all concentrations.

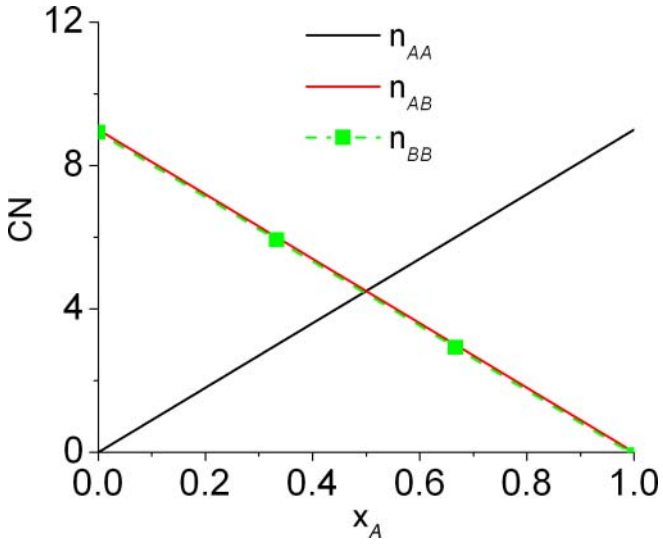

Fig. 5. Theoretical partial coordination numbers in random nanoalloys (assuming $n_{MM} = 9$) as a function of composition.

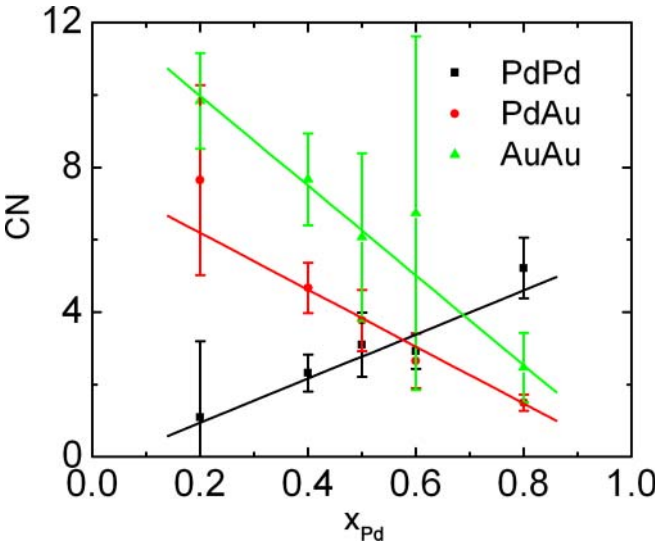

Fig. 6. Experimentally obtained partial coordination numbers in dendrimer-stabilized PdAu nanoparticles as a function of composition. The alloying is quasi-random.

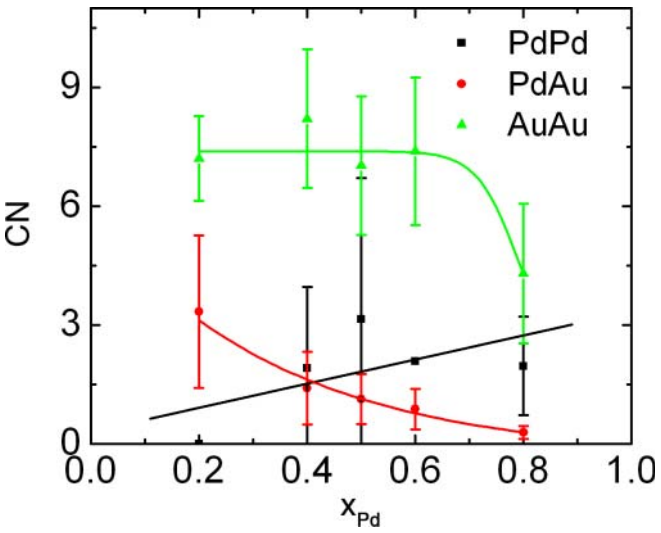

Fig. 7. Experimentally obtained partial coordination numbers in monolayer-protected PdAu nanoparticles as a function of composition. The curves are guides to the eye. The alloying is consistent with Pd segregating to the shell, Au – to the core of the nanoparticles.

Knecht, *et al.* [28], demonstrated that a dendrimer-stabilized system of Pd−Au nanoparticles with narrow size distribution (~147 atoms, *i.e.*, $n_{MM} = 8.98$, assuming the perfect cuboctahedral model) does behave as a quasi-random alloy throughout the entire concentration range (Fig. 6). Monolayer-protected clusters of the same size showed a different behavior, consistent with Pd-rich shell and Au-rich core at all concentrations (Fig. 7).

EXAFS and heterogeneity

After background subtraction and edge-step normalization of the raw absorption coefficient, resultant EXAFS $\chi(k)$ corresponds to an "average" single atom absorption. The averaging of the local pair distribution functions $\varrho(r)$ around all absorbing atoms is obtained automatically in the process of data measurement and reduction: first, the contributions of each absorber's environments are added by measuring total absorption coefficient, and, at the next stage, are weighted by the molar fractions of absorbing atoms in each species during the edge step normalization:

$$\varrho(r) = \sum_{s=1}^{n} x_s \varrho^{(s)}(r), \tag{9}$$

where

$$x_s = \frac{N_s}{N}; \qquad \sum_{s=1}^{n} x_s = 1.$$

In Eq. (9), N is the total number of absorbing atoms, $n$is the total number of species, N_s is the total number of absorbing atoms in species s. Equation (9) is valid both for the entire r-range of the RDF as well as for the range corresponding to a specific atomic shell within $[r, r + \Delta r]$. Their applications to the coordination numbers of each shell are straightforward:

$$n_{ME_i} = x_s \frac{N_{ME_i}}{N_s} = x_s n^{(s)}_{ME_i}, \qquad E_i \neq M, \tag{10}$$

$$n_{MM} = x_s \frac{2N_{MM}}{N_s} = x_s n^{(s)}_{MM}, \qquad E_i = M, \tag{11}$$

where N_{ME_i} is the total number of $M-E_i$ pairs. The factor of two in the bottom line of Eq. (11) is due to the fact that each atom of the $M-M$ pair is an absorber and thus the number of these pairs should be doubled in calculating the $M-M$ coordination numbers. Note that, since the mixing fractions x_s are constants that contribute to the amplitude of EXAFS, they correlate only with coordination numbers n_{ME_i}. The nearest neighbor distances R_{ME_i} and their disorders $\sigma^2_{ME_i}$ are calculated the same way for heterogeneous and homogeneous mixtures. Note also that Eqs. (10) and (11) are a generalization from the case of a homogeneous mixture (where each absorber's environment is chemically equivalent), in which case $x_s = 1$. Since $n^{(s)}_{ME_i}$ denotes a partial coordination number of $M-E_i$ within the volume occupied by the species s, it is this parameter that characterizes the local environment of M in this species, not the overall n_{ME_i} measured by EXAFS. For a homogeneous system, $n^{(s)}_{ME_i} = n_{ME_i}$. For a heterogeneous mixture, however, since $N_s < N$, $n^{(s)}_{ME_i} > n_{ME_i}$. Therefore, if the possibility of segregation of the absorbing atoms to chemically different environments is not accounted for in the analysis, the size of the nanoparticles will be underestimated. Since such information is not available from EXAFS, it should be combined with other methods for analysis of heterogeneous systems, as demonstrated below.

Consider a common scenario in nanocatalysis where a sample is a mixture of two species: (1) reduced monometallic nanoparticles and (2) molecular precursors, mixed with fractions x_1 and x_2, respectively. Typical EXAFS data of an analogous system of dodecanethiolate Pd nanoparticles coexisting with Pd sulfide molecular complexes [29] are shown in Fig. 8.

As in most compounds where EXAFS data in r-space have two split peaks due to the $M-$O (or C, N, S etc.) and $M-M$ contributions, the data in Fig. 8 has two contri-

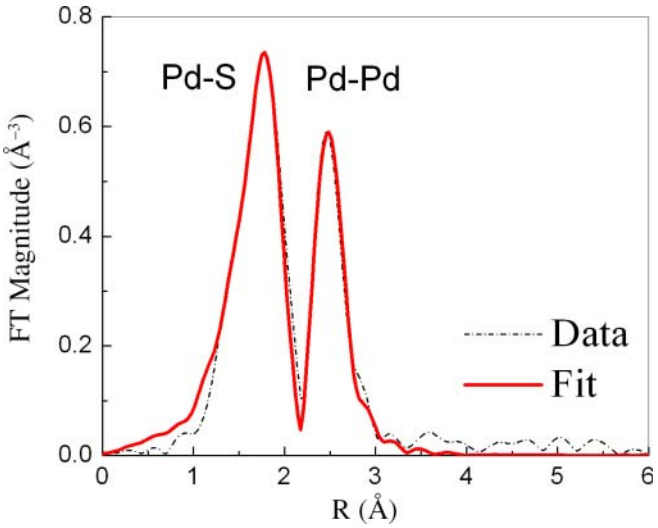

Fig. 8. Data and FEFF6 fit of dodecanethiolate Pd nanoparticle system.

butions: Pd−S and Pd−Pd that can be separately quantified by EXAFS analysis. The Pd−S and Pd−Pd coordination numbers were obtained by EXAFS analysis [29] $n_{\mathrm{Pd-S}} = 2.2 \pm 0.4$ and $n_{\mathrm{Pd-Pd}} = 4.0 \pm 0.9$. The interpretation of these results depends critically on the independent knowledge of the state of heterogeneity of the system. Assuming a homogeneous model, this result corresponds to a hypothetical system with ca. four Pd−Pd and two Pd−S bonds per Pd atom. Evidently, such clusters should have fewer atoms than 13 if only symmetric, closed-shell, three-dimensional clusters are considered. Indeed, for a closed packed, 13-atom clusters, $n_{MM} = 5.54$, and for the 13-atom icosahedron it is larger: 6.46 [22]. However, TEM measurements indicated much larger clusters (26 ± 8 Å in diameter) [22], corresponding to the average coordination number of 10.05 if a cuboctahedral ($L = 5$, *i.e.*, 6 atoms on the edge) model is assumed, with experimentally meausured Pd−Pd 1 NN distance of 2.74 Å. Assuming a two-component system, we obtain that $x = n_{\mathrm{Pd-Pd}}/n^{(s)}_{\mathrm{Pd-Pd}} \approx 40\%$ Pd atoms can be found in clusters and 60% – in Pd-sulfide complexes. If EXAFS data quality is sufficiently high, the presence of large particles may be indicated by EXAFS signal at high r (Fig. 8), *i.e.*, originating from distant neighbors and multiple-scatterings.

We would like to emphasize that in the above example only the combination of these complementary methods, TEM and EXAFS, allowed to obtain such level of detail about the local structure of a heterogeneous system. However, in the situation where the mixing fractions in a multi-component mixture change as a function of some external factor (*e.g.*, time, in the case of an isothermal chemical reaction, or potentiostatic control in the case of electrochemical reduction/oxidation, or pH, etc.), the number and identities of the constituent species, and their mixing fractions as a function of time, potential, pH etc., may be obtained by a Principal Component Analysis (PCA) of XANES or EXAFS data [30].

Acknowledgments. This work was supported by the U.S. Department of Energy Grant No DE-FG02- 03ER15476. The author would like to thank L. M. Menard and M. Knecht for useful discussions, and access to well characterized nanoparticle samples with exceptional size and compositional control, as well as D. Glasner for writing a suite of programs for cluster geometry generation and S. Calvin for useful comments.

References

[1] Briant, C. E.; Theobald, B. R. C.; White, J. W.; Bell, L. K.; Mingos, M. P.: Synthesis and *X*-ray structural characterization of the centred icosahedral gold cluster compound $[Au_{13}(PMe_2Ph)_{10}Cl_2](PF_6)_3$; the realization of a theoretical prediction. J. Chem. Soc., Chem. Comm. (1981) 201–202.

[2] Petkov, V.; Peng, Y.; Williams, G.; Huang, B.; Tomalia, D.; Ren, Y.: Structure of gold nanoparticles suspended in water studied by X-ray diffraction and computer simulations. Phys. Rev. B**72** (2005) 195402–195410.

[3] Singhal, A.; Yang, J. C.; Gibson, J. M.: STEM-based mass spectroscopy of supported Re clusters. Ultramicroscopy **67** (1997) 191–206.

[4] Li, Z. Y.; Yuan, J.; Chen, Y.; Palmer, R. E.; Wilcoxon, J. P.: Direct imaging of core-shell structure in silver-gold bimetallic nanoparticles. Appl. Phys. Lett. **87** (2005) 243103–243106.

[5] Menard, L. D.; Gao, S.-P.; Xu, H.; Twesten, R. D.; Harper, A. S.; Song, Y.; Wang, G.; Douglas, A. D.; Yang, J. C.; Frenkel, A. I.; Nuzzo, R. G.; Murray, R. W.: sub-nanometer Au monolayer protected clusters exhibiting molecule-like electronic behavior: Quantitative HAADF-STEM and electrochemical characterization of clusters with precise atomic stoichiometry. J. Phys. Chem. B**110** (2006) 12874–12883.

[6] Kang, J.; Menard, L. M.; Frenkel, A. I.; Nuzzo, R. G.: Unusual non-bulk properties in nanoscale materials: thermal metal-metal bond contraction of gamma-alumina-supported Pt catalysts. J. Am. Chem. Soc. (Communications) **128** (2006) 12068–12069.

[7] Sayers, D. E.; Lytle, F. W.; Stern, E. A.: New Technique for Investigating Noncrystalline Structures: Fourier Analysis of the Extended X-Ray – Absorption Fine Structure. Phys. Rev. Lett. **27** (1971) 1204–1207.

[8] Lytle, F. W.; Via, G. H.; Sinfelt, J. H.: New application of extended X-ray absorption fine structure (EXAFS) as a surface probe-nature of oxygen interaction with a ruthenium catalyst. J. Chem. Phys. **67** (1977) 3831–3832; Sinfelt, J. H.; Via, G. H.; Lytle, F. W.: Extended X-ray absorption fine structure (EXAFS) of supported platinum catalysts. J. Chem. Phys. **68** (1977) 2009–2010; Meitzner, G.; Via, G. H.; Lytle, F. W.; Sinfelt, J. H.: Structure of bimetallic clusters. Extended X-ray absorption fine structure (EXAFS) studies of Rh–Cu clusters. J. Chem. Phys. **78** (1983) 882–889; Meitzner, G.; Via, G. H.; Lytle, F. W.; Sinfelt, J. H.: Structure of bimetallic clusters. Extended X-ray absorption fine structure (EXAFS) of Pt−Re and Pd−Re clusters. J. Chem. Phys. **87** (1987) 6354–6363.

[9] Zabinsky, S. I.; Rehr, J. J.; Ankudinov, A.; Albers, R. C.; Eller, M. J.: Multiple-scattering calculations of X-ray-absorption spectra. Phys. Rev. B **52** (1995) 2995–3009.

[10] Newville, M.: IFEFFIT: interactive XAFS analysis and FEFF fitting. J. Synchrotron Rad. **8** (2001) 322–324.

[11] Arratia-Perez, R.; Ramos, A. F.; Malli, G. L.: Calculated electronic structure of Au_{13} clusters. Phys. Rev. B**39** (1989) 3005–3009.

[12] Cleveland, C. L.; Landman, U.; Schaaff, T. G.; Shafigullin, M. N.; Stephens, P. W.; Whetten, R. L.: Structural evolution of smaller gold nanocrystals: The truncated decahedral motif. Phys. Rev. Lett. **79** (1997) 1873–1876.

[13] Cleveland, C. L.; Landman, U.; Shafigullin, M. N.; Stephens, P. W.; Whetten, R. L.: Structural evolution of larger gold clusters. Z. Phys. D**40** (1997) 503–508.

[14] Köhn, A.; Weigend, F.; Ahlrichs, R.: Theoretical study of clusters of magnesium. Phys. Chem. Chem. Phys. **3** (2001) 711–719.

[15] Brack, M.: The physics of simple metal clusters: self-consistent jellium model and semiclassical approaches. Rev. Mod. Phys. **65** (1993) 677–732.

[16] Zhang, Z.; Hu, W.; Xiao, S.: Shell and subshell periodic structures of icosahedral nickel nanoclusters. J. Chem. Phys. **122** (2005) 214501–214501-5.

[17] Cortie, M. B.; van der Lingen, E.: Catalytic gold nanoparticles. Mater. Forum **26** (2002) 1–14.

[18] Montejano-Carrizales, J. M.; Aguilera-Granja, F.; Moran-Lopez, J. L.: Direct enumeration of the geometrical characteristics of clusters. NanoStructured Mater. **8** (1997) 269–287.
[19] Calvin, S.; Miller, M. M.; Goswami, R.; Cheng, S.-F.; Mulvaney, S. P.; Whitman, L. J.; Harris, V. G.: Determination of crystallite size in a magnetic nanocomposite using extended X-ray absorption fine structure. J. Appl. Phys. **94** (2003) 778–783.
[20] Frenkel, A. I.: Solving the structure of nanoparticles by multiple-scattering EXAFS analysis. J. Synchrotron Rad. **6** (1999) 293–295.
[21] Frenkel, A. I.; Hills, C. W.; Nuzzo, R. G.: A view from the inside: complexity in the atomic scale ordering of metal nanoparticles. J. Phys. Chem. B (Feature Article) **105** (2001) 12689–12703.
[22] Glasner, D.; Frenkel, A. I.: Geometrical characteristics of regular polyhedra: Application to EXAFS studies of nanoclusters. AIP Conf. Proc. **882** (2007) 746–748.
[23] Menard, L. D.; Xu, H.; Gao, S.-P.; Twesten, R. D.; Harper, A. S.; Song, Y.; Wang, G.; Douglas, A. D.; Yang, J. C.; Frenkel, A. I.; Murray, R. W.; Nuzzo, R. G.: Structural dynamics of ultrasmall monolayer protected clusters: Metal core bonding motifs of monodispersed icosahedral Au_{13} and larger Au nanoparticles as revealed by X-ray absorption spectroscopy and transmission electron microscopy. J. Phys. Chem. B**110** (2006) 14564–14573.
[24] Frenkel, A. I.; Menard, L. D.; Northrup, P.; Rodriguez, J. A.; Zypman, F.; Glasner, D.; Gao, S.-P.; Xu, H.; Yang, J. C.; Nuzzo, R. G.: Geometry and charge state of mixed-ligand Au_{13} nanoclusters. AIP Conf. Proc. **882** (2007) 749–751.
[25] Hwang, B.-J.; Sarma, L. S.; Chen, J.-M.; Chen, C.-H.; Shih, S.-C.; Wang, G.-R.; Liu, D.-G.; Lee, J.-F.; Tang, M.-T.: Structural models and atomic distribution of bimetallic nanoparticles as investigated by X-ray Absorption Spectroscopy. J. Am. Chem. Soc. **127** (2005) 11140–11145.
[26] Cowley, J. M.: Short-range order and long-range order parameters. Phys. Rev. **138** (1965) A1384–A1389.
[27] Nashner, M. S.; Frenkel, A. I.; Adler, D. L.; Shapley, J. R.; Nuzzo, R. G.: Structural characterization of carbon supported Pt–Ru nanoparticles from the molecular cluster precursor $PtRu_5C(CO)_{16}$. J. Am. Chem. Soc. **119** (1997) 7760–7771.
[28] Knecht, M. R.; Meir, M. G.; Frenkel, A. I.; Crooks, R. M.: Structural rearrangement of bimetallic alloy PdAu nanoparticles to yield core/shell configurations. Chem. Mater. (2007) in press.
[29] Sun, Y.; Frenkel, A. I.; Isseroff, R.; Schonbrun, C.; Forman, M.; Shin, K.; Koga, T.; White, H.; Zhang, L.; Zhu, Y.; Rafailovich, M. H.; Sokolov, J. C.: Characterization of Palladium Nanoparticles by Using X-ray Reflectivity, EXAFS, and Electron Microscopy. Langmuir **22** (2006) 807–816.
[30] Frenkel, A. I.; Kleifeld, O.; Wasserman, S.; Sagi, I.: Phase speciation by extended X-ray absorption fine structure spectroscopy. J. Chem. Phys. **116** (2002) 9449–9456; Rodriguez, J. A.; Hanson, J. C.; Frenkel, A. I.; Kim, J.-Y.; Perez, M.: Experimental and Theoretical Studies on the Reaction of H_2 with NiO: Role of O Vacancies and Mechanism for Oxide Reduction. J. Am. Chem. Soc. **124** (2002) 346–354; Kim, Y.; Rodriguez, J. A.; Hanson, J. C.; Frenkel A. I.; Lee P. L.: Reduction of CuO and Cu_2O with H_2: H embedding and kinetic effects in the formation of suboxides. J. Am. Chem. Soc. **125** (2003) 10684–10692; Wang, X.; Hanson, J. C.; Frenkel, A. I.; Kim, J.-J. ; Rodriguez, J. A.: Time-resolved studies for the mechanism of reduction of copper oxides with carbon monoxide: complex behavior of lattice oxygen and the formation of suboxides. J. Phys. Chem. B**108** (2004) 13667–13673; Kleifeld, O.; Frenkel, A. I.; Martin, J. M. L.; Sagi, I.: Metal site electronics and dynamics during metalloenzyme catalysis. Nat. Struct. Biol. **10** (2003) 98–103.